Size-induced metal insulator transition and glassy magnetic behavior in La 0.5 Sr 0.5 Co O 3 nanoparticles

B. Roy and S. Das

Citation: Applied Physics Letters **92**, 233101 (2008); doi: 10.1063/1.2943188
View online: http://dx.doi.org/10.1063/1.2943188
View Table of Contents: http://scitation.aip.org/content/aip/journal/apl/92/23?ver=pdfcov
Published by the AIP Publishing

Size-induced metal insulator transition and glassy magnetic behavior in $La_{0.5}Sr_{0.5}CoO_3$ nanoparticles

B. Roy[1] and S. Das[2,a)]
[1]*Department of Physics, Ramakrishna Mission Vidyamandira, Belur Math, Howrah 711 202, India*
[2]*ECMP Division, Saha Institute of Nuclear Physics, 1/AF Bidhannagar, Kolkata 700 064, India*

(Received 15 April 2008; accepted 16 May 2008; published online 9 June 2008)

Structural, electrical, and magnetic properties of $La_{0.5}Sr_{0.5}CoO_3$ nanoparticles prepared by sol-gel technique are investigated and the results reveal a size-induced metal insulator transition in the electrotransport behavior. The field cooled and zero field cooled magnetizations display a broad paramagnetic to ferromagnetic transition at T_c with a large magnetic irreversibility. Attempts are made to get an idea about the spin states in the nanoparticles. The observed frequency dependent shoulder in the in-phase (χ') component and the peak in the out of phase (χ'') component of the ac susceptibility in the low temperature region indicate the glassy nature of the samples. © *2008 American Institute of Physics*. [DOI: 10.1063/1.2943188]

$LaCoO_3$ with Co^{3+} ($3d^6$) ions is a charge transfer-type insulator with no magnetic order. The substitution of Sr^{2+} for La^{3+} in $LaCoO_3$ converts Co^{3+} to Co^{4+} and the magnetic properties of cobaltites depend on the spin states of Co^{3+} and Co^{4+} ions. Ferromagnetic (FM) ordering appears due to the double exchange interactions between Co^{3+} and Co^{4+} ions. In $La_{1-x}Sr_xCoO_3$, Co ions (Co^{3+} and Co^{4+}) have six different spin states (low, intermediate, and high), among which transitions take place by a change in external stimuli such as temperature or pressure. The spin state transition originates from a competition between the crystal field splitting energy and the intra atomic Hund exchange coupling energy. Theoretical calculations reveal that strong hybridization between ligand O $2p$ and Co $3d$ orbitals stabilizes the intermediate spin (IS) state with the introduction of holes in the oxygen $2p$ orbital. Due to very small energy difference between the spin states, the variation in temperature drives a gradual switch over from low spin (LS) to IS or high spin (HS) state for both the Co^{3+} and Co^{4+} ions. From magnetic relaxation studies on $La_{1-x}Sr_xCoO_3$, Itoh *et al.*[1] suggested that cluster-glass properties exist in the region $(0.18 \leqslant x < 0.5)$ due to the random distribution of Sr and the competition between the FM double-exchange interaction between Co^{4+} and Co^{3+} and antiferromagnetic superexchange interaction between the HS states such as $Co^{3+}-Co^{3+}$ and $Co^{4+}-Co^{4+}$. Recently, research on nanocrystalline materials has attracted much attention due to their interesting properties. In this letter we report the modifications in structural, electrical, and magnetic properties of $La_{0.5}Sr_{0.5}CoO_3$ nanoparticles with the change in particle dimensions.

Nanoparticles of $La_{0.5}Sr_{0.5}CoO_3$ were prepared following the citrate gel process.[2] The size was determined from the x-ray diffraction (XRD) peak width using Scherrer's formula modified by Williamson and Hall[3] and also by transmission electron microscopic (TEM) measurements. The temperature dependence of electrical resistivity was measured by the standard four probe method. Magnetic properties of the samples have been studied using a Quantum Design MPMS5 superconducting quantum interference device with the magnetic field from 10 Oe to 50 KOe. The XRD patterns show that all the samples are in single phase. A representative plot of XRD pattern of the 21 nm sample along with its refined pattern is shown in Fig. 1. The XRD data are refined, using Rietveld FULLPROF program,[4] assuming a rhombohedral structure with the $R\bar{3}C$ space group symmetry. The refined parameters of all the samples are computed and included in Table I. The results show that the unit cell parameters increase, bond length decreases, and bond angle enhances as the particle size increases. The average particle size and the lattice strain are calculated using the Williamson–Hall method. In this method, the experimental x-ray peak broadening is given by $\beta = K\lambda/t \cos\theta + 2\epsilon \tan\theta$, where β is the full width at half maximum of the XRD peaks, θ is the Bragg angle, K is the particle shape factor (=0.89), λ is the wavelength of Cu $K\alpha$ radiation, and ϵ is the strain in the sample. A plot of $\beta\cos\theta$ versus $\sin\theta$ is a straight line, shown in the inset of Fig. 1. The average crystalline size (t) is calculated from the intercept of the straight line with the vertical axis (Table I) while the slope of the straight line gives the lattice stain (ϵ). A typical TEM image

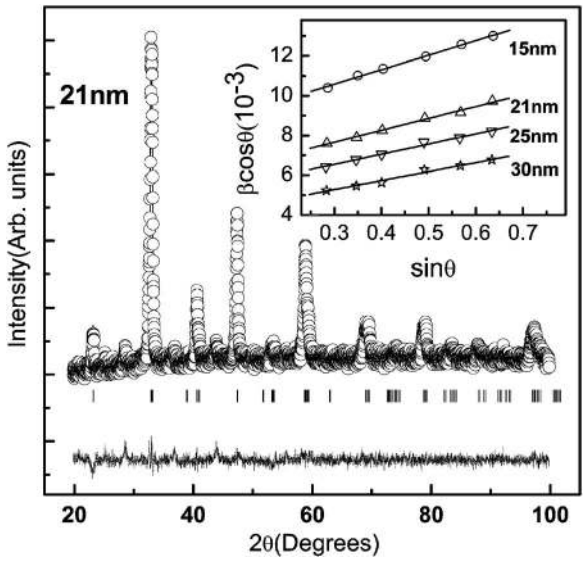

FIG. 1. The plot of the Rielveld refinement of the XRD data of the 21 nm sample. Inset shows the Williamson–Hall plot for various samples.

a)Electronic mail: sailendranath.das@saha.ac.in.

TABLE I. Particle size from XRD and TEM, annealing temperature (T_{ann}), refined x-ray structural parameters, various characteristics temperatures, and effective magnetic moments.

Particle size (nm)		T_{ann}	a	c	Co–O–Co	d_{Co-O}	T_c	δT_c	T_{irr}	Θ	μ_{eff}
XRD	TEM	(°C)	(Å)	(Å)	(degree)	(Å)	(K)	(K)	(K)	(K)	(μ_B)
18.8	15	650	4.7029	13.1694	168.117	1.928	190	30	189	215	2.37
22.5	21	700	4.7133	13.2049	168.251	1.926	225	23	218	239	2.59
26.3	25	775	4.7153	13.2496	168.710	1.925	242	10	230	247	3.81
30.4	30	850	4.7174	13.2612	168.824	1.924	245	8	236	249	3.96

of the 21 nm sample is shown in Fig. 2. It should be noted from the table that the average size obtained from the TEM study are slightly different from the crystalline size estimated from the XRD measurement due to the presence of lattice strain which influences the XRD peaks. From Fig. 3 it is evident that a size-induced metal to insulator transition takes place with a semiconducting nature for the 15 and 21 nm samples and metallic for the rest. The resistivity of the semiconducting compounds increases with the decrease in particle size, implying that decrease in grain size relatively increases the insulating regions due to the enhancement in the grain boundary effect. The low temperature part of the resistivity can be explained in the light of thermally activated type hopping model of conductivity. The resistivity data in the paramagnetic (PM) region fits very well with the adiabatic small-polaron hopping equation[2] $\rho = BT\exp(E_\rho/k_BT)$, where E_ρ is the activation energy. In both the cases the values of activation energy decrease as the particle size increases. For metallic samples (Fig. 3) $\rho(T)$ is almost linear in T above the FM transition (T_c) but changes its slope with an increase in conduction just below T_c. The latter is due to the reduction in scattering of electrons from spin disorder as the compounds undergo PM to FM transition. The resistivity data of the 30 and 25 nm samples in the FM states can be fitted using the formula[2] $\rho(T) = \rho_0 + \rho_2 T^2 + \rho_{4.5} T^{4.5}$, where ρ_0 is the residual resistivity, ρ_2 is the electron-electron scattering, and $\rho_{4.5}$ is the magnon scattering coefficients. The increase in ρ_0 indicates that the cluster boundary scattering increases with a decrease in size.

The zero field cooled (ZFC) and field cooled (FC) magnetization [Fig. 4(a)] show a large thermomagnetic irreversibility with irreversibility temperature (T_{irr}) being close to T_c. The maximum in the $M_{ZFC}(T)$ curve is observed at a temperature lower than T_{irr}. The large difference between the FC and ZFC magnetization indicates that the samples have short-range FM interactions. This behavior has been associated with one of the characteristic features of the cluster glass system.[1,5] T_c was determined by the minimum of the dM/dT versus T curves (Table I). The width of transition (δT_c) increases with the decrease in particle size. This broad transition suggests a possible existence of a wide distribution of exchange interactions in the vicinity of the grain boundaries. In the PM regime, the samples obey the Curie–Wiess law [Fig. 4(b)]. The PM Curie temperature (Θ) steadily decreases with a decrease in size (Table I). To elucidate the spin states of the cobalt ions in the nanoparticles, the effective magnetic moment μ_{eff} is calculated from the linear part of the Curie–Wiess regime. The value of the effective magnetic moment μ_{eff} decreases with decreasing size. In $La_{0.5}Sr_{0.5}CoO_3$ system, the total spin can be expressed as $S_{spin} = 0.5S_3 + 0.5S_4$, where S_3 and S_4 represent the spin of Co^{3+} and Co^{4+} ions, respectively. Recent studies have suggested that the Co^{3+} ions are in the IS state in $La_{1-x}Sr_xCoO_3$ compounds, but the spin state of Co^{4+} ions is still an open issue. It could be in the LS, IS, HS or a mixture of these states.[6] If we assume that in the 30 nm sample Co^{3+} ions are in the IS($S_3=1$) state but the Co^{4+} ions are in the IS($S_4=1.5$) and HS($S_4=2.5$) states in the ratio of 2:3, the effective magnetic moment is calculated by using the formula $\mu_{eff} = g[J(J+1)]^{1/2}\mu_B$, and considering the spin only value (i.e., $J = S_{spin}$), we get $\mu_{eff} = 3.97\mu_B$. In consistence with the previous reports[1,7,8] the spin distribution in the higher dimensional

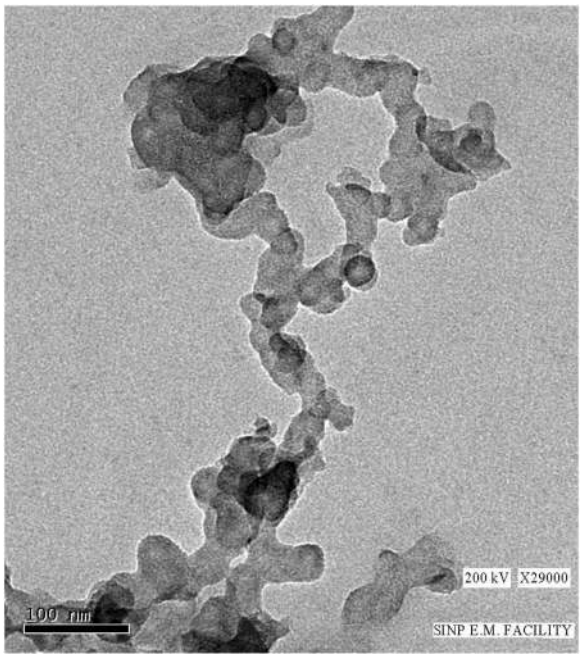

FIG. 2. Transmission electron micrograph of the 21 nm sample.

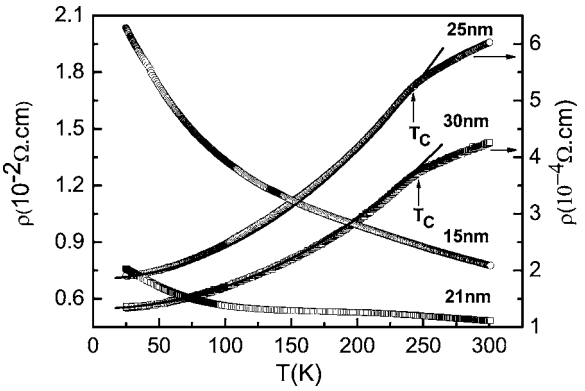

FIG. 3. Temperature dependence of resistivity. Solid lines give the best fit to $\rho(T) = \rho_0 + \rho_2 T^2 + \rho_{4.5} T^{4.5}$ in the metallic region.

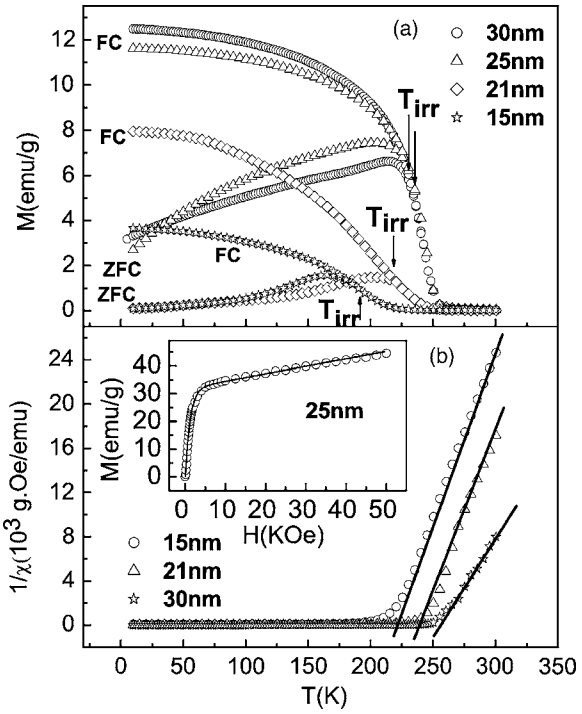

FIG. 4. (a) FC and ZFC dc magnetization of $La_{0.5}Sr_{0.5}CoO_3$ samples as a function of temperature under a magnetic field of 200 Oe. (b) $1/\chi$ vs T for the 15, 21, and 30 nm samples; solid lines represents the fit to the Curie–Weiss law. The inset shows the variation in magnetization of the 25 nm sample with field at 5 K. The solid line is the best fit line obtained by fitting with $M(H)=NgJ\mu_B B_J(x)+\chi_0 H$.

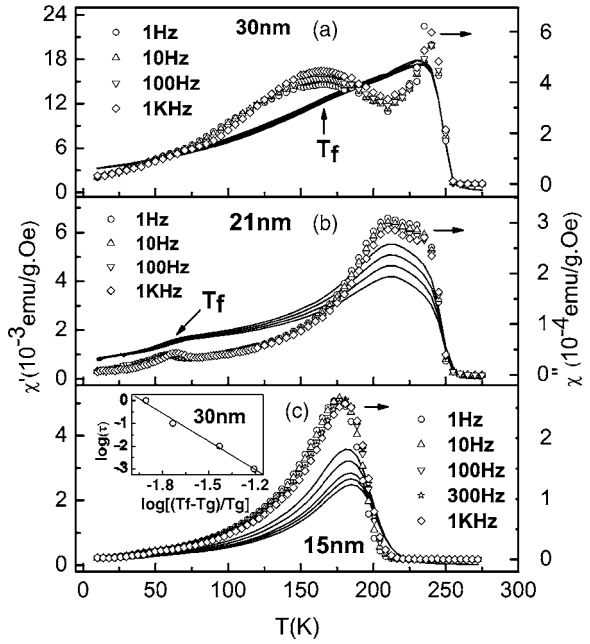

FIG. 5. Temperature dependence of χ' and χ'' at different frequencies for the (a) 30 nm, (b) 21 nm, and (c) 15 nm samples. Inset of (c) shows the $\log(\tau)$ vs $\log[(T_f-T_g)/T_g]$ curve with best fit line.

sample shows a good agreement between experimental and theoretical results. The inset of Fig. 4(b) shows the magnetization (M) versus magnetic field at temperature 5 K for the 25 nm sample. In order to estimate the spin state of this sample we have fitted the data with the following expression[9] $M(H)=NgJ\mu_B B_J(x)+\chi_0 H$, $(x=J\mu_B H/k_B T)$, where N is the number of clusters with the effective spin J per unit mass, $B_J(x)$ the Brillouin function, and χ_0 is the coefficient of the linear term. The best fit is obtained for $J=1.55$. It suggests that the spin configuration in the 25 nm sample is similar to that of the 30 nm sample. Figure 4(a) shows that magnetization decreases due to the enhancement in the surface disorder with the decrease in particle size. In that case the above mentioned explanation should also consider the surface-core model of nanoparticles.[2]

From the in-phase component of the ac susceptibility $\chi'(T)$ (Fig. 5), the high temperature maximum is found to be frequency independent and it shifts to low temperature with a decrease in size. The shoulder at T_f shifts to low temperature and finally disappears as size decreases. From Fig. 5 it is also observed that the high temperature peak position in the out of phase component of ac susceptibility $\chi''(T)$ shifts to low temperature with the decrease in particle size. For the 30 and 21 nm samples, the high temperature peak in $\chi''(T)$ appears at the same temperature as that in the $\chi'(T)$ curve but they have different origins. The high-temperature peak in $\chi''(T)$ is related to the irreversibility temperature (T_{irr}) in dc $M(T)$. It should be noted that the shoulder in the $\chi'(T)$ curves and a peak in $\chi''(T)$ appeared at almost the same temperature (T_f). The temperature (T_f) increases with increasing excitation frequency (f). The low temperature peak may be attributed to the freezing of the FM clusters. The peak clearly shifts to low temperature and the intensity of the peak is greatly reduced with the decrease in particle size. The freezing temperature can be obtained from the frequency dependence of T_f. We have estimated the freezing temperature (T_g) by extrapolating the T_f versus frequency curve to zero frequency. The frequency dependence can be well described by invoking the critical slowing down of the spin dynamics[6] expressed as $\tau/\tau_0=[(T_f-T_g)/T_g]^{-z\nu}$, where τ is the relaxation time $\propto f^{-1}$, τ_0 is the characteristic time constant, and $z\nu$ is a critical exponent. The best fit to $\log(\tau)$ versus $\log[(T_f-T_g)/T_g]$ curve, shown in the inset of Fig. 5(c), gives $\tau_0=10^{-8}$ s, 5.14×10^{-9} s, and $T_g=162$, 53 K, $z\nu=4.13, 7.46$ for the 30 and 21 nm samples, respectively. Thus, the ac susceptibility measurement supports the cluster glass nature of $La_{0.5}Sr_{0.5}CoO_3$ nanoparticles.

[1]M. Itoh, I. Natori, S. Kubota, and K. Motoya, J. Phys. Soc. Jpn. **63**, 1486 (1994).
[2]B. Roy, A. Poddar, and S. Das, J. Appl. Phys. **100**, 104318 (2006).
[3]K. Williamson and W. H. Hall, Acta Metall. **1**, 22 (1953).
[4]J. Rodriguez-Carvajal, Physica B **192**, 55 (1993).
[5]D. N. H. Nam, K. Jonason, P. Nordblad, N. V. Khiem, and N. X. Phuc, Phys. Rev. B **59**, 4189 (1999).
[6]J. Wu and C. Leighton, Phys. Rev. B **67**, 174408 (2003).
[7]K. Yoshii and H. Abe, Phys. Rev. B **67**, 094408 (2003).
[8]X. Xu, L. Jiang, J. Shen, Z. Chen, and Z. Xu, Phys. Lett. A **351**, 431 (2006).
[9]S. Yamaguchi, Y. Okimoto, H. Taniguchi, and Y. Tokura, Phys. Rev. B **53**, R2926 (1996).